Catalysis Science & Technology

Accepted Manuscript

ROYAL SOCIETY OF CHEMISTRY

www.rsc.org/catalysis

Insights into the effects of steam on propane dehydrogenation over Pt/Al_2O_3 catalyst

Yu-Ling. Shan[1], Yi-An Zhu[1], Zhi-Jun. Sui[1,*], De Chen[2] and Xing-Gui Zhou[1]

[1]State Key Laboratory of Chemical Engineering, East China University of Science and Technology, Shanghai 200237, P. R. China

[2]Department of Chemical Engineering, Norwegian University of Science and Technology, N-7491, Trondheim, Norway

Corresponding author:zhjsui@ecust.edu.cn

Abstract

Catalytic propane dehydrogenation over an alumina supported Pt catalyst in the presence of steam is carried out and it is found that the catalyst activity is increased and the apparent activation energy lowered due to the presence of steam. Three possible mechanisms, i.e. co-adsorption, Langmuir-Hinshelwood and Eley-Rideal, of changes in energetics and pathways for propane dehydrogenation due to the presence of steam are explored by DFT calculation. The results show that co-adsorption of C_3 species with the surface oxygenated species would elevate dehydrogenation energy barriers due to repulsion interactions between them. Surface –OH is more active than surface –O in activating C-H bond in propane and propyl species through either Langmuir-Hinshelwood or Eley-Rideal mechanism and plays an important role in propane dehydrogenation with steam. The Langmuir-Hinshelwood mechanism is kinetically favorable, in which the activations of the first H in propane by surface -OH are the rate determining steps, but the activation energies are higher than that on clean Pt(111) surface. The observed enhanced catalyst's activity is ascribed to the lowered coking rates as well as the changes in surface coverage due to the co-adsorption of

water and the surface oxygenated species.

Keywords: propane dehydrogenation; steam; DFT calculations; Pt catalyst; reaction mechanism;

1 Introduction

Propene is an important building block for a wide range of commodity and specialty chemicals[1-4]. Now, traditional ways of producing it can no longer meet the ever growing need. As the natural gas supplies are increasing due to the rising exploration of shale gas[5], there has been growing interest in recent years in the on-purpose production of propene from propane dehydrogenation (PDH) technologies. Tens of PDH factories with total capacity of over 10 million of tons are building all over the world[6].

Supported platinum catalyst is used in several commercialized PDH technologies[7], e.g. Oleflex, STAR, etc. and proved by experimental and theoretical studies to be the most active catalyst for PDH due to its high density of electronic states close to the Fermi level[8, 9,10]. Large research efforts have been devoted to trying to promote the performances of Pt catalysts by introducing promoters or using different kinds of supports[11-13]. But coking and deactivating of this kind of catalyst are still inevitable problems[14].

In industrial practice, co-feed of hydrogen[7,15-18] or steam[19] with propane is used to enhance the performance of platinum-based catalysts. The presence of hydrogen can contribute to higher propene selectivity and lower coking rate[15-17]. Using DFT

calculation, Hauser *et al.*[20] and Yang *et al.*[21] have proved that the presence of surface hydrogen atom can shift the third C-H cleavage step to a higher value, making it less competitive to the preferred alkene desorption step and thus improve the dehydrogenation selectivity at the cost of elevating activation energies. However, introducing hydrogen in the PDH process seem to be unfavorable from engineering point of view since it would decrease the equilibrium conversion and increase the compression energy consumption for the following separation process.

Steam has been widely used as energy carrier, coke remover and diluent in dehydrogenation processes[19, 22, 23]. Introducing steam in the feed can strengthen PDH processes by increasing propane equilibrium conversion and lowering the temperature drop of the adiabatic dehydrogenation reactors[19]. Dong *et al.*[24] found that under the same propane partial pressure, steam can contribute to higher propene yield compared with that in nitrogen atmosphere. However, the results reported by Fattahi *et al.*[25] and our group[26] have shown that the promoting effect of steam on PDH over alumina supported Pt-Sn catalyst is only valid in a certain range of steam amount.

For the purpose of taking the best advantage of those merits of steam, several terms should be addressed. For one thing, platinum-based catalysts used in steam atmosphere need to be designed carefully to avoid the sintering of Pt particles[27,28]. Beyond this, the critical role of steam on dehydrogenation kinetics over Pt surfaces should be illustrated to help to determine the optimum operating conditions and provide some insight into the basic principles for catalysts design. Unfortunately, these questions are still poorly understood and consensus has hardly been reached. In

the kinetic model for PDH in steam atmosphere developed by Luu *et al.*[29] over a tin modified Pt/γ -Al_2O_3, steam was involved in the dominator of their kinetic model with a second order. But to interpret similar retarding effects of steam, some other authors[25,27,28] suggested that sintering of platinum particles was the reason for the observed activity decrease. Several authors[25, 28, 30] in literature also suggested that surface hydroxyl generated from adsorption and dissociation of water may help to remove hydrogen in the rate limiting step of propane dehydrogenation and thus increase propene formation rate. Unfortunately, this hypothesis has not been verified by either experimental or theoretical results.

In the present study, the effect of steam on PDH has been re-examined over a monometallic Pt catalyst with narrow particle size distribution. To obtain additional insights into the effect of steam on PDH over Pt nanoparticles, a computational study has also been carried out, focusing on the influence of surface adsorbate, like H_2O, hydroxyl group (–OH) and oxygen atom (–O), on the C-H bond activation.

2 Experimental detail

Alumina supported platinum catalyst was prepared by the colloid method[31]. The preparation procedures were as follows. Firstly, 5 mL water and 5 mL ethylene glycol were mixed in a flask. Then 2.0 g of γ-Al_2O_3 (Aldrich) and 0.1 g of H_2PtCl_6•$6H_2O$ (99.9%, Sinopharm) was added and dispersed with the help of ultra-sonic wave. After stirring overnight, the pH of the solution was adjusted to 13.0 by using sodium hydroxide in non-aqueous ethylene glycol (2M). After that, the platinum was reduced at 130 ^{o}C in argon for 4 h, then cooled to room temperature and the pH of the solution

was adjusted to 3.0. After stirring another 2 h, the solids were obtained after subsequent repeated centrifugation, washing and drying processes.

The metal loading of the catalyst was determined by ICP-AES and the metal dispersion was characterized by H_2-Chem and HRTEM techniques. The PDH reaction was carried out in a μBenchCAT reactor (Altamira Instrument, USA) equipped with a quartz reactor with an inner diameter of 6 mm. The reactor was placed in an electrical furnace and the reaction temperature can be maintained within ±0.5 ^{o}C of the desired set point. The catalyst loading was 0.05g for all catalyst testing experiments. All the experiments were conducted at $WHSV_{propane}$ = 7.1 h^{-1} and a hydrogen to propane molar ratio of 4. The water was introduced into the reactor system by using a pump and vaporized before reaching the reaction zone. Argon was used as balance gas to get a total flow of 200 ml/min. The mass transfer limitations were excluded at these conditions. The gas composition (C_1-C_3 hydrocarbons, H_2, CO and CO_2) were analyzed online with a 4-channel Micro-GC(INFICON*3000, USA*).

3. Computational details

Periodic density functional theory (DFT) calculations have been carried out using the VASP package[32-34]. The generalized gradient approximation (GGA) with the PBE functional was used for all the atoms. The interactions between valence electrons and ion cores were represented by Blöchl's all-electron-like projector augmented wave method (PAW)[35]. A tight convergence of the plane-wave expansion was obtained with a cut-off of 400 eV. Brillouin zone sampling was performed by using a Monkhorst–Pack grid with respect to the symmetry of the system and the electronic

occupancies were determined according to a Methfessel-Paxton scheme[36] with an energy smearing of 0.2 eV.

The Pt(111) surface was represented by a four-layer slab with a p(3×3) supercell, as described previously[37]. A Monkhorst–Pack mesh of 7×7×1 *k*-points was used for the 2D Brillouin zone integration. The bottom two layers of the slab were kept fixed to their crystal lattice positions (Pt-Pt distance = 2.82 Å). Spin-polarization had been considered for radical-containing systems. The ground-state atomic geometries of bulk and surfaces were obtained by minimizing the Hellman–Feynman forces with the conjugate-gradient algorithm until the total force on each ion was below 0.03 eV/Å. The adsorption energy (E_{ads}) was calculated according to the expression

$$E_{ads} = E_{adsorbate/substrate} - E_{adsorbate} - E_{substrate} \qquad (1)$$

where E_X is the DFT-total energy of the X system. A negative E_{ads} indicates an energy gain process.

Transition states (TS) were searched with the dimer method[38-40]. The most stable configurations of the reactant on the surface were determined by the sta ndard DFT minimization. These configurations were used as the initial state, from which the dimer method was used to find the lowest curvature mode and to climb up the potential energy surface from minima to saddle points. The convergence was regarded to be achieved when the force on each atom was less than 0.03 eV/Å.

4. Results

4.1 Experimental results

The physical properties of the prepared Pt/γ-Al_2O_3 catalyst are as follows. The platinum loading of it is 1.5% and the mean particle size is 4.9 nm, based on H_2-Chem results (metal dispersion of 23.3 %), which is comparable to the statistics result of 5.5 nm obtained from HTEM images, shown in Fig. S1(Supporting Information).

Propane dehydrogenation over this catalyst was performed to investigate the effect of steam. During the experiments, the conversion of propane was found to be within 7.0%, thus the turnover frequency ($TOF_{(propane,\ propylene)}$) to represent the catalyst's activity can be calculated as following :

$$TOF_{propane} = \frac{\text{mole of propane conversion}}{\text{mole of surface atoms of catalyst} \times \text{reaction time}}$$

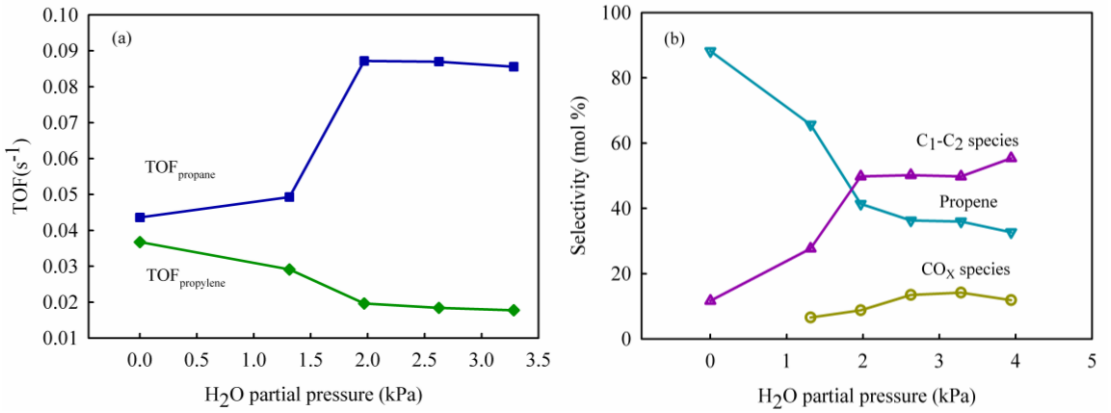

Fig. 1 Activity and selectivity to products for PDH over Pt(EG) catalyst at different H_2O partial pressure, recorded at 1.5minute later after feed in. Condition: $C_3H_8/H_2/H_2O/Ar$=3/12/X/(100-X), X is shown in picture , 450 ^oC.

As is shown in Fig. 1(a), the catalyst's activity ($TOF_{propane}$) increases with the increase of steam partial pressure and reaches a plateau at higher steam concentrations, which may indicate that the reaction is controlled by water adsorption equilibrium under these water partial pressures. At the same time, the opposite trend is observed for the propene formation rates and the gap between $TOF_{propane}$ and $TOF_{propylene}$

increases with the increase of steam partial pressure and finally reaches a plateau as well. When looking into products distribution, it can be seen from Fig. 1(b) that the loss of the selectivity to propylene mainly goes to the cracking products, CH_4 and C_2H_4, with a selectivity of around 60.0% at steam partial pressure of between 1.92 and 3.5 kPa. In the same steam partial pressure range, oxidizing products, CO and CO_2, are also detected with the selectivity to them of around 10.0%, indicating the dissociation of water and the involvement of these oxygenated species in propane dehydrogenation pathways.

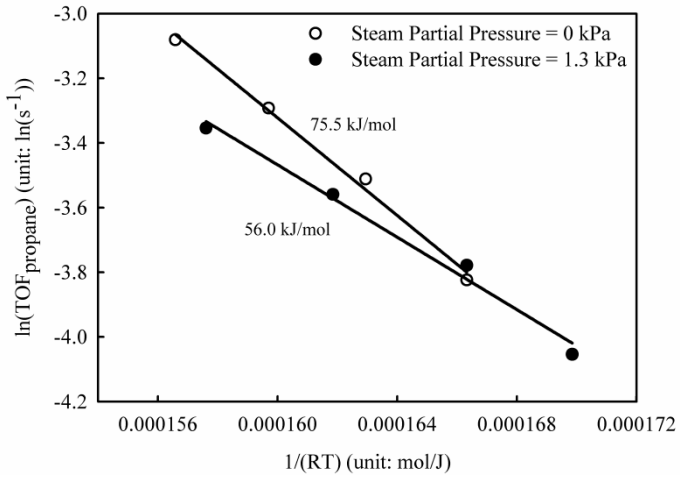

Fig. 2 Apparent activation energies for PDH under different conditions. Condition: C_3H_8, 1.5 kPa; H_2, 6 kPa, steam partial pressure is shown in picture, balance is nitrogen.

The apparent activation energies under different conditions were evaluated and presented in Fig. 2. It is found that PDH in the presence of steam has lower activation energies of 56.0 kJ/mol than that without steam introduction of 75.5 kJ/mol. The activation energies obtained here fit in the range of 30-150 kJ/mol for PDH reported in Ref[41].

From results stated above, it can be seen that introduction of steam in the feed has apparent and complicated influences on PDH over Pt catalyst, which testifies the

essential role of water and surface oxygenated species in the PDH. But whether the participation of these surface oxygenated species would alter the reaction route and thus decrease the PDH apparent activation energy or not is still under debate. In the following parts, DFT investigation of the effect of adsorption of steam and its subsequent dissociated species on PDH reaction mechanism is conducted and the factors contributing to changes in catalyst's performance are discussed.

4.2 DFT results

We started with the co-adsorption of C_3 species and water. Then, three possible changes in dehydrogenation mechanisms were considered in the following parts: 1) Dehydrogenation of C_3 species over oxygenated species pre-covered Pt(111) surfaces (Co-adsorption effects for short hereafter); 2) Dehydrogenation of C_3 species over Pt(111) surfaces with the participation of surface oxygenated species in the transition states for dehydrogenation and hydrogen removal (Langmuir-Hinshelwood mechanism); 3) Dehydrogenation of C3 species over the adsorbed surface oxygenated species (Eley-Rideal mechanism).

4.2.1 Co-adsorption with water

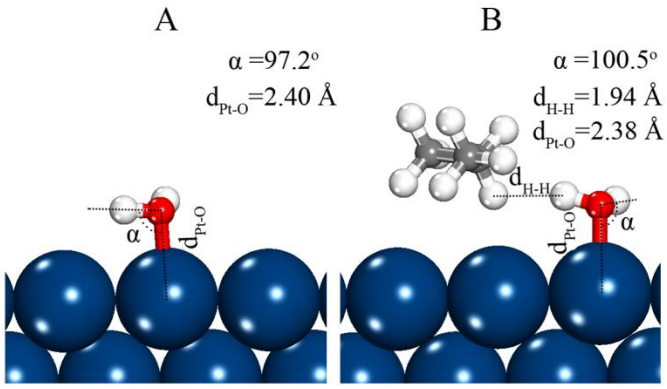

Fig.3 Structures of the adsorbed water and propane in the presence of water

The adsorptions of water monomer and co-adsorption of water and C3 species were studied to explore possible existing interactions between them. The adsorption configurations with lowest-energy for water monomer and water-propane complex were presented in Fig. 3. A water monomer favorably adsorbs on atop sites of Pt(111) surface via an O-Pt bond of 2.40 Å and α_{HO} (HOH plane orientation over the surface) of 97.2°, which are in consistent with DFT calculations in literatures[42-44] and indicate that water is nearly parallel to the surface. For the water-propane complex, the nearest H-H bond between them is 1.94 Å. Changes in water structure are observed that the O-Pt bond is shortened by 0.02 Å and the angle of α_{HO} increases by 3.2°. But no noticeable changes in configurations of propane compared with that on clean surface could be observed.

The calculated adsorption energies are listed in table 1. To better understand the interaction between the hydrocarbon species and water, the co-adsorption energies are decomposed according to the following function:

$$E_{ads\_A} + E_{ads\_B} = E_{coads} + E_{int\_AB} \qquad (2)$$

where E_{ads_A}/E_{ads_B} is one-point adsorption energy of A or B by fixing their geometries, E_{int_AB} is the interaction energy between A and B, E_{coads} is the overall co-adsorption energy of A-B complex, A and B represent hydrocarbon species and water, respectively.

In the case of water-propane complex, no noticeable changes in adsorption energy of propane (E_{ads_A}) and water (E_{ads_B}) is observed. The increased E_{coads} is ascribed to the existing of a weak attractive interaction between propane and water

(0.05 eV in strength). But for *n*-propyl, *i*-propyl and propene, co-adsorption with water result in a decrease of E_{coads} (0.06 and 0.08 eV in strength, respectively) due to repulsion interactions between them. It also should be noticed that, in the case of propene-water co-adsorption, significant decrease of E_{ads_B} was observed (decreased by 0.05 eV), indicating changes of water adsorption configuration in addition to the repulsion interaction.

Table 1. Co-adsorption energies of some intermediates for propane dehydrogenation in the presence of surface H_2O.

Species	E_{coads}	E_{ads_A}		E_{ads_B}		E_{int_AB}
	(eV)	Clean	coads	clean	coads	
C_3H_8 & H_2O	-0.21	-0.04	-0.04	-0.12	-0.12	0.05
n-C_3H_7 & H_2O	-2.03	-1.98	-1.98	-0.12	-0.11	−0.06
i-C_3H_7 & H_2O	-1.82	-1.81	-1.80	-0.12	-0.10	−0.08
C_3H_6 & H_2O	-1.14	-1.12	-1.11	-0.12	-0.07	−0.04

4.2.2 Co-adsorption effects

The presence of carbon oxides as by-products indicates the dissociation of water molecule on platinum surface. Therefore, surface -OH and -O are also considered in the following parts to investigate the possible influences of them on dehydrogenation mechanism. In this section, the co-adsorption effects are discussed.

The most favorable adsorption sites for surface -OH and -O are bridge and hollow sites, respectively, as listed in table S1. To search for the transition states for dehydrogenating steps, surface -OH or -O was put at different favorable adsorption

sites adjacent to dehydrogenated species and the ones with the most stable configurations were selected. The results were listed in Table 2.

Table. 2 Activation energies for dehydrogenation over clean and oxygenated species pre-adsorbed Pt(111) surface.

	Elementary Steps	Pt^{37}	H_2O*Pt	OH*Pt	O*Pt
ES1	$CH_3CH_2CH_3* \rightarrow CH_3CH_2CH_2 + H*$	0.69	0.72	0.75	0.74
ES2	$CH_3CH_2CH_3* \rightarrow CH_3CHCH_3 + H*$	0.70	0.73	0.74	0.74
ES3	$CH_3CH_2CH_2* \rightarrow CH_3CHCH_2 + H*$	0.70	0.72	0.76	0.75
ES4	$CH_3CHCH_3* \rightarrow CH_3CHCH_2 + H*$	0.68	0.69	0.76	0.73
ES5	$CH_3CHCH_2* \rightarrow CH_3CHCH + H*$	0.76	0.81	0.79	0.87
ES6	$CH_3CHCH_2* \rightarrow CH_3CCH_2 + H*$	0.77	0.82	0.83	0.86

As can be seen from Table 2, co-adsorption of water and oxygenated species with C3 species could elevate all the activation energies of different elementary steps to some extent. For example, with the co-adsorption of water, the activation energies of propane dehydrogenation to propene (ES1-ES4 in Table2) are elevated slightly by 0.01~0.03 eV; in the cases of co-adsorption with surface -OH and -O, the activation energies of ES1-ES4 steps are lifted by 0.05~0.06 eV. The elevation of the activation energies for dehydrogenation steps indicates that the catalyst activity may decrease for the co-adsorption mechanism. Among all the three co-adsorption species, co-adsorption of water has the least influence on PDH energy barriers, but the discrepancies from the effect of the other two species is small. Considering the fact that the structures of transition states remain almost unchanged compared with that on clean surface (shown in Fig. S2), the repulsion between surface oxygenated species

and C3 species would account for such increase in activation energy.

The activation energies of propene deep dehydrogenating steps (ES5 and ES6) are elevated by 0.03-0.11 eV due to the presence of co-adsorption species indicating the co-adsorption mechanism may decrease the catalyst activities. But, it should be noticed that this may not mean the selectivity to propene cracking reactions is reduced. Actually, for the co-adsorption of surface –OH, the difference between the ES5 and ES1-ES4 is reduced, indicating the relative reaction rate of propene dehydrogenation/propane dehydrogenation may increase and the selectivity to propene will decrease due to the existence of this species.

4.2.3 Langmuir-Hinshelwood mechanism

The Langmuir-Hinshelwood mechanism is discussed in this section. For the convenience of comparison, the related results of propane dehydrogenation on bare Pt(111) surfaces[37] are recalled.

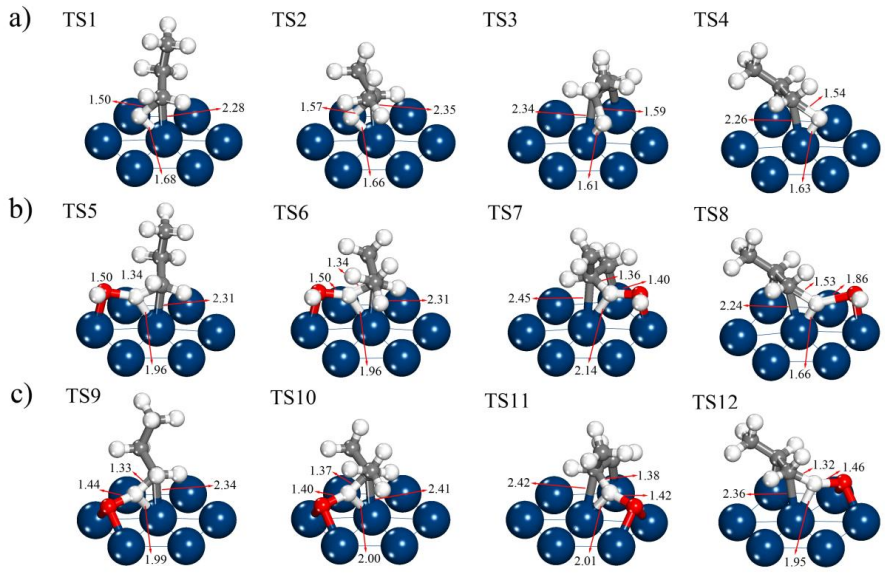

Fig. 4 Transition states structures of propane dehydrogenation at a) clean Pt(111) surface, b) OH*Pt(111) surface, c) O*Pt(111) surface.

The structure configurations for propane dehydrogenation on bare Pt(111) surface are presented in Fig. 4(a). For the first C-H bond activation, through primary H (TS1) or secondary H atom (TS2), the readily removing H atom is adsorbed on bridge sites of Pt surface, with C-H bond length of 1.50 Å and 1.57 Å, respectively. When an adsorbed hydroxyl is presented at atop of the adjacent Pt atom, it can be involved in the TS (TS5 and TS6 in Fig. 4(b)) by interacting with the readily removing H atom. These structures give shorter C-H bond length of 1.34 Å, meanwhile, a water molecule is nearly formed with a H-O bond length of 1.50 Å. Similar TS structures can be obtained in the case of surface oxygen atom (TS9 and TS10 in Fig. 4(c)), in which oxygen atom is adsorbed at bridge site on Pt surface and a surface hydroxyl is to be formed.

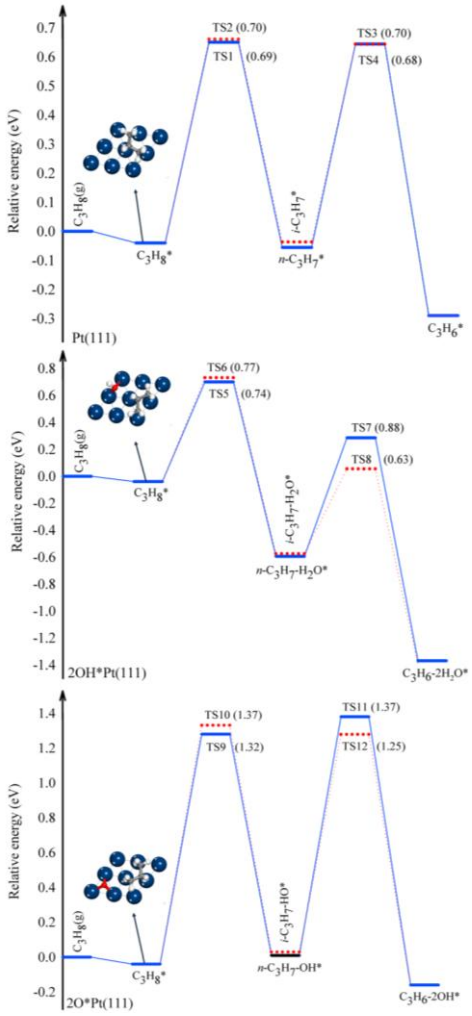

Fig. 5 Reaction paths of propane dehydrogenation to propene: (1) at the clean platinum surface Pt(111), (2) at the hydroxylated surface OH*Pt(111), (3) at the oxygenated surface O*Pt(111). Energies are in eV.

The activation energies for these dehydrogenation steps are presented in Fig. 5. For activation of the first H atom, the results show that the involvements of hydroxyl in TS structures shift the energy barriers to higher values of 0.74 eV (TS5) and 0.77 eV (TS6) to produce *n*, *i*-propyl species, respectively, compared with those of 0.69 eV (TS1) and 0.70 eV (TS2) on bare Pt(111) surface. Moreover, the surface -O involved steps have even higher activation energies of 1.32 eV (TS9) and 1.37 eV (TS10), suggesting the inactive nature of these surface oxygen atoms. The distance of H-Pt

bond in these cases are elongated by around 0.3 Å, which indicates the decrease of adsorption energy due to the repulsion interaction between the surface oxygenated species and adsorbed C3 species and could partly account for the higher activation energies of these steps.

Interesting phenomenon was found in the case of surface -OH assisted β-H elimination steps. At the TS8, through which *i*-propyl dehydrogenates to propene, the activated C-H bond length (1.53 Å) is similar to that on bare surface (1.54 Å) and the H-O bond (1.86 Å) is longer than that in TS5-TS7 (1.40-1.50 Å). This configuration gives an activation energy of 0.63 eV, lower than that on bare surface by a magnitude of 0.05 eV. But, for surface -OH assisted *n*-propyl dehydrogenating to propene, the activation energy is elevated to 0.88 eV. Surface -O is also inactive in the β-H elimination steps. As can be seen from Fig. 6, the activation energies of these steps are elevated to as high as 1.25~1.37 eV(TS 11 and TS12), which are much higher than that of 0.68-0.70 eV(TS3 and TS4) on bare Pt(111) surfaces.

Table. 3 Decomposition of the activation energy for propane dehydrogenation (step 2) on Pt(111) and OH*Pt(111)

Reaction Path	$E_{ads,TS}$	$E_{ads,TS}$ (propene)	$E_{ads,TS\ (H)}$	$E_{int,lat}$ (H,propene)	$E_{ads,TS}$ (OH)	$E_{int,lat}$ (OH,propene+H)
Through TS3	-2.93	-0.79	-2.62	0.48	-	-
Through TS7	-5.09	-0.20	-1.57	-0.73	-2.14	-0.45
Through TS4	-2.96	-0.82	-2.2	0.48	-	-
Through TS8	-5.38	-0.90	-2.61	0.54	-2.23	-0.18

To provide a rational interpretation for the obtained results, the activation energies for propene producing steps are decomposed as follows:

$$E_{act} = E_{ads,TS} - E_{bond(C_3H_6-H)} - E_{ads,C_3H_7} \quad (3)$$

where $E_{ads,TS}$ is the adsorption energy of the activated complex with respect to the gaseous propene , OH and H species , $E_{bond(C3H6-H)}$ is the C−H bond energy at the methyl group of gaseous *n*-propyl or *i*-propyl and $E_{ads,C3H7}$ is the adsorption energy of propyl species. As the bond energy and propyl adsorption energy keep constant, the variation in E_{act} depends solely on the changes in $E_{ads,\ TS}$ which can be further decomposed into the following five terms:

$$E_{ads,TS} = E_{ads,TS(propene)} + E_{ads,TS(H)} + E_{ads,TS(OH)} + E_{int,lat(H,propene)} + E_{int,lat(H+propene,OH)} \quad (4)$$

where $E_{ads,TS(propene)}$, $E_{ads,TS(H)}$, $E_{ads,TS(OH)}$ are the adsorption energies of propene, H and OH respectively with their geometries in the activated complex, $E_{int,lat(H,propene)}$ and $E_{int,lat(H+propene,\ OH)}$ represents the interaction energy of H-propene and OH-(H+propene) in the activated complexes respectively. From Eq 4, one can see that a more negative $E_{ads,TS(propene)}$ ($E_{ads,TS(H)}$, $E_{ads,TS(OH)}$) and a lower $E_{int,lat(H,propene)}$ ($E_{int,lat(H+propene,\ OH)}$) lead to a more negative $E_{ads,TS}$, which contribute to a lower energy barrier.

The transition states of TS3 and TS4 on bare Pt(111) surface and their counterparts of surface -OH assisted ones TS7 and TS8 are decomposed to analyze the factors contributing to the elevated and lowered activation energies. The results are shown in Table 3. In TS7, it is found that the adsorptions of propene and hydrogen are weakened, hydroxyl can attract hydrogen with an attractive energy of -0.45 eV and the interaction between hydrogen and propene is lowered. But the interactions are

insufficient to compensate the weakened adsorption of hydrocarbons and shift the activation energy to a higher value. In TS8, the attractive energy from surface -OH is lower than that in TS7, but the adsorption energies for propene and hydrogen are higher than those on bare Pt(111) surface and lower the activation energy. This means that the adsorption energies of propene and hydrogen atom dominates in the activation energies.

When the total energy of the initial propane and -OH (or –O) co-adsorption state is set to zero, it can be seen that the surface -OH assisted dehydrogenation route is thermodynamically favorable with heat releases of 0.59 eV and 0.77 eV for the two consecutive C-H bond activation steps. While the situation is different for surface oxygen atom involved reactions, in which the first step is a slightly endothermic reaction and only the second step is an exothermic step with a releasing heat of 0.16 eV. Therefore, the surface oxygen atom is both kinetically and thermodynamically unfavorable.

4.2.4 Eley-Rideal mechanism

It's well known that catalytic oxidative dehydrogenation of propane over some metal oxide catalysts follows Mars-van Krevelen mechanism[45-49] and Eley-Rideal mechanism[50-53], for the later pathways, the surface oxygen species are involved in activating and abstracting H from propane. To gain a better understanding of the effect of oxygenated species on Pt(111) surface, this possible reaction pathway is also considered here.

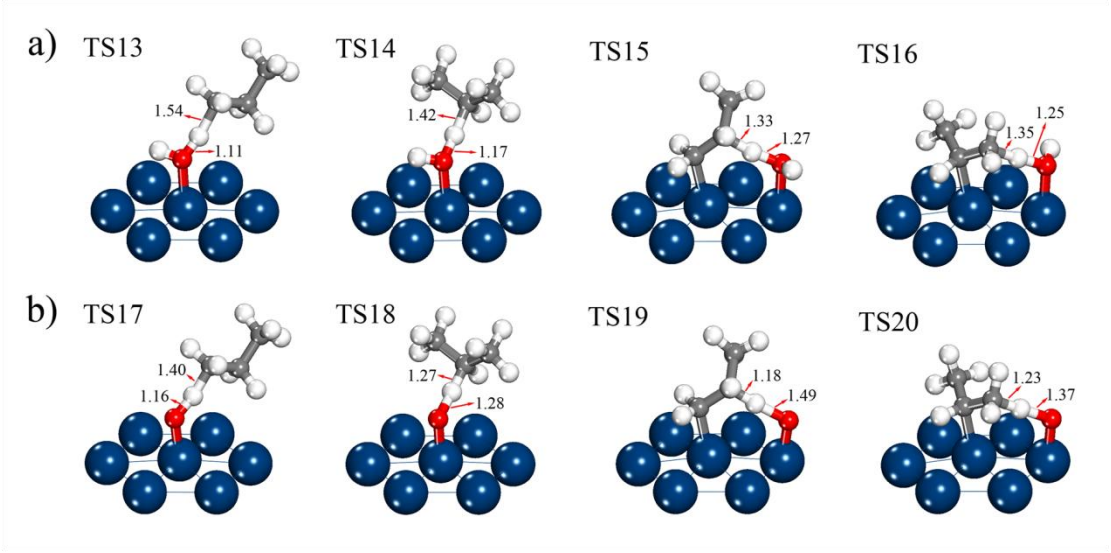

Fig. 6 Transition states structures of propane oxidative dehydrogenation at a) OH*Pt(111) surface, b) O*Pt(111) surface.

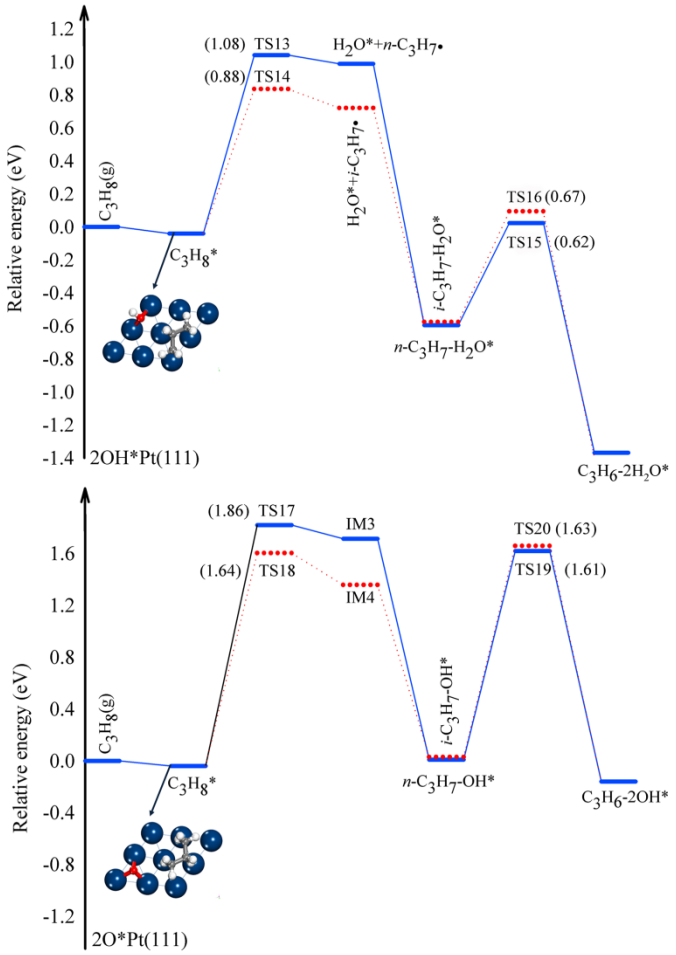

Fig. 7 Reaction pathways of oxidative dehydrogenation on: a) OH*Pt(111) surface, b) O*Pt(111) surface.

Fig. 6 shows the transition states of H atom abstraction by surface oxygenated

species and the corresponding energy profiles are shown in Fig. 7. In the case of oxidation of propane by surface hydroxyl through H abstraction, the transition state for the activation of the C-H bond in methyl group is successfully located and presented in Fig.6 of TS13, in which the C-H bond is elongated from 1.10 Å to 1.54 Å and a water molecule is readily formed with a H-O distance of 1.11 Å, which is quite close to the H-O bond length of 0.99 Å in a gaseous H_2O molecule. The reaction barrier is calculated to be 1.08 eV. The activation of propane through the breaking of C-H bond in methylene was also calculated and found to be more favorable with an energy barrier of 0.88 eV. Shorter C-H bond length of 1.42 Å can be observed in the geometry. From thermodynamic points of view, the C-H bond energy in methyl group is stronger than that in the methylene group (420 kJ/mol and 401 kJ/mol[54]). Therefore, the production of *i*-propayl radical is both thermodynamically and kinetically favored, which is in consistence with the observations in the literature[46, 54, 55].

For oxidation of propane by atomic oxygen species, the energy barrier of producing *i*-propyl radical is 0.22 eV lower than that of producing *n*-propyl radical and kinetically favorable. However, compared with dehydrogenation by surface hydroxyl, the activation of propane by atomic oxygen species is much harder since producing *i*-propyl radical needs to conquer an energy barrier of as high as 1.64 eV. The atop site for oxygen atom adsorption in transition states is one of the reasons accounting for such high activation energy. The most favored adsorption configuration for oxygen atom is hollow sites with adsorption energy of 4.41 eV and adsorption on atop sites has adsorption energy of 3.13 eV. But the transition states

cannot be successfully located when putting oxygen at either hollow or bridge sites.

After the first H abstraction from propane, propyl radicals are formed in the gas phase (as shown in Fig. 8). These radicals are close to the newly formed groups (surface H_2O or -OH) with bond lengths ranging from 1.99 Å to 2.18 Å. At the next step, these radicals will adsorb on Pt(111) surface, and no transition states could be located for the adsorption processes.

The β-hydrogen elimination steps can also proceed by the H abstracting reaction in the presence of surface oxygenated species and this step follows surface reaction mechanism. The transition states are successfully located and the specific configurations are shown in Fig. 6 of TS15, TS16, TS19, and TS20. The activated C-H bonds are shorter than these involved in the first hydrogen activation in propane, as shown in Fig. 6, and the newly formed H-O bonds are longer accordingly. It's apparent that lower energies are needed to activate the second hydrogen, especially in the surface hydroxyl involved reactions, and the activation energies are even lower than that on clean Pt(111) surface.

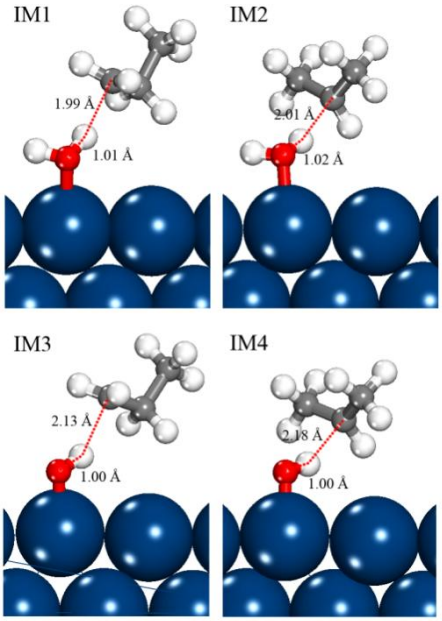

Fig. 8 Intermediates formed on hydroxylated and oxygenated platinum surfaces.

When dehydrogenation of propane by surface hydroxyl and oxygen atom are compared, it is found that the first H abstraction reactions are the rate limiting steps in both cases, which is in consistence with results obtained by DFT studies for oxidative dehydrogenation of propane over vanadium oxide[54-56] but differs from dehydrogenation of propane over Pt(111) surface[37]. Surface hydroxyl is more active than atomic oxygen species from the kinetic point of view since lower energy barrier is needed to break C-H bond. Moreover, the consecutive two H abstracting reactions by surface hydroxyl are all exothermic. So it is also thermodynamically more favorable than dehydrogenation by surface O. But, among all the three mechanism discussed above, the essential role of surface –OH is achieved most likely through Langmuir-Hinshelwood mechanism, since the activation energies for this mechanism have the relative low values.

5. Discussion

The increase of catalytic activity and decrease of apparent activation energies are

observed in experiments when introducing steam in the PDH reaction. But the DFT results stated above shows that co-adsorbing with oxygenated species can shift the activation energies to higher values due to the repulsion among the co-adsorption species. For the Langmuir-Hinshelwood mechanism, the activations of the first C-H bonds in propane are not facilitated because of stereospecific blockade. In some specific steps, e.g. *i*-propyl dehydrogenating to propylene, surface –OH can help to activate C-H bond of methyl group due to the electronic interactions. For Eley-Rideal mechanism, although the second step of C-H bond activation by surface –OH is slightly kinetically favored, the first step of C-H bond abstraction gives high energy barriers of 0.88 eV and 1.08 eV for *i*-propyl and *n*-propyl radical producing, respectively. Therefore, the DFT results do not seem to support the conclusion of alternation in reaction pathways for PDH in the presence of steam.

It should be noticed that adsorption of water on the Pt surface would change the surface coverage of different species and therefore affect the reaction rate. For PDH over Pt catalyst, Chen et al[57]. found the reaction order to hydrogen is -0.5, which indicates that lower hydrogen partial pressure and surface coverage will lead to the increase of the reaction rate. This phenomenon is also supported by the previous DFT results[21]. But, the water adsorption on Pt(111) is weak and may have a low surface coverage, which would limit the effect of steam in a certain range. As is shown in Fig.9, hydrogen order to PDH reaction remains nearly unchanged in steam atmosphere since the hydrogen order to PDH reaction can be expressed as follows[31]:

$$n_{H_2} = -\theta_H - 0.5$$

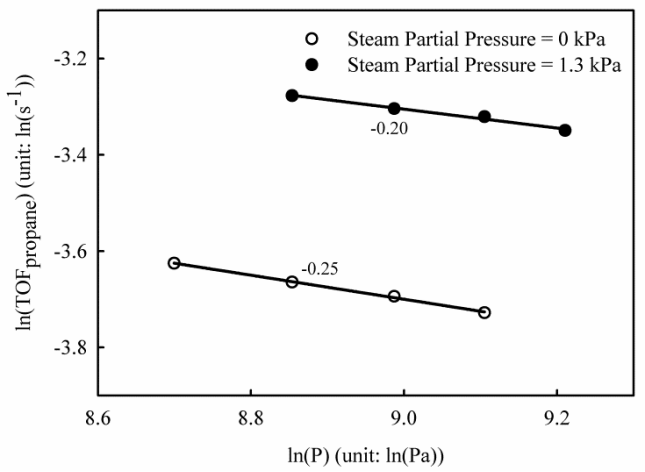

Fig. 9 Reaction order to hydrogen for PDH under different conditions. Condition: C3H8, 1.5 kPa; H2, 6 kPa.

Table 4. Coking rates under different steam partial pressures

H_2O Partial Pressure (KPa)	Reaction Time (h)	Coking Rate ($g_{coke}/(g_{Pt}•s)$)
0.00	1	8.23e-5
1.31	1	7.29e-5
1.95	1	7.14e-5
2.63	1	6.86e-5
3.28	1	6.77e-5

Another advantages of steam for PDH is that steam could contribute to lower coking rate[25,58,59], which is justified by our TG analysis of the spent catalysts, as shown in Table 4. The decrease of coking rate in the presence of steam contributes to the increase of catalytic activity, since more Pt(111) surface may be free for the reaction[21]. Furthermore, It should be noted that when steam is introduced, the selectivity loss of propene mainly goes to cracking products, in accordance with other authors[28,60]. Yang et al[37,61] and Nykänen et al[62] have shown that lower coordinated Pt sites, like step sites, are highly active but are not selective for PDH reaction. On these

sites, cracking products and coking reaction prevail. Therefore, mono-metallic Pt catalysts suffer from rapid deactivation[15, 63-66]. When steam is introduced, the removal of cokes will help recover and maintain these highly active Pt sites and increase the catalyst's activity and decrease the selectivity to propene at the same time. Since propane dehydrogenation on these sites have lower activation energies[37, 62], it can also account for the experimentally observed decrease in activation energies[67].

Finally, it should be noted that the change of propane dehydrogenation activities is also related to the catalysts structures. It was found by Luu et al[29] that steam was involved in the dominator of their kinetic model with a second order over tin promoted Pt/γ-Al_2O_3, indicating that H_2O was adsorbed on active sites. But for their Pt/γ-Al_2O_3 catalyst without tin addition, the dehydrogenating rates were hardly dependent on the partial pressure of steam, revealing that the effects of steam might depend on different support[24,67] and catalysts' composition[24,29,67].

6. Conclusion

A combined experimental and theoretical study of the effect of steam on propane dehydrogenation was performed. The experimental results show that addition of steam in the PDH reaction will increase the catalyst's activities, lower dehydrogenating activation energies and coking rate. Compared with dehydrogenation over clean Pt(111) surface, the DFT results show that the energy barriers of different dehydrogenation steps are elevated due to the adsorption of water and its dissociated species. The only exception is for *i-propyl* dehydrogenating to propene step with the involvement of surface -OH through both Langmuir-Hinshelwood and Eley-Rideal

mechanism. For PDH under steam atmosphere, the role of surface –OH is essential, most likely through Langmuir-Hinshelwood mechanism, in which the first C-H bond activation is the rate determining step in the overall PDH reaction route. The promoting effect of steam can be ascribed to the removal of cokes deposited on active Pt surfaces and the changes of adsorption species coverage on Pt surface.

Acknowledgement

This work is supported by the National Basic Research Program of China (973 project, 2012CB720500), the Fundamental Research Funds for the Central Universities of China (222201313006, WA1414043), National Science Foundation of China (91434117，21376076) and the 111 project(B08021).

References

1. R. J. Rennard and J. Freel, *J. Catal.*, 1986, 98, 235-244.
2. S. Derossi, G. Ferraris, S. Fremiotti, E. Garrone, G. Ghiotti, M. C. Campa and V. Indovina, *J. Catal.*, 1994, 148, 36-46.
3. M. Fattahi, M. Kazemeini, F. Khorasheh and A. M. Rashidi, *Catal. Sci. Technol.*, 2015, 5, 910-924.
4. Q. Li, Z. Sui, X. Zhou and D. Chen, *Appl. Catal. A- Gen.*, 2011, 398, 18-26.
5. E. McFarland, *Science*, 2012, 338, 340-342.
6. J. J. H. B. Sattler, J. Ruiz-Martinez, E. Santillan-Jimenez and B. M. Weckhuysen, *Chem. Rev.*, 2014, 114, 10613-10653.
7. B. Vora, *Top. Catal*, 2012, 55, 1297-1308.
8. J. K. Norskov and F. Abild-Pedersen, *Nature*, 2009, 461, 1223-1225.
9. A. T. Bell, *Science*, 2003, 299, 1688-1691.
10. L. Nykänen and K. Honkala, *J. Phys. Chem. C*, 2011, 115, 9578-9586.
11. A. Iglesias-Juez, A. M. Beale, K. Maaijen, T. C. Weng, P. Glatzel and B. M. Weckhuysen, *J.Catal.* 2010, 276, 268-279.
12. G. Siddiqi, P. Sun, V. Galvita and A. T. Bell, *J.Catal.*, 2010, 274, 200-206.
13. P. Sun, G. Siddiqi, W. C. Vining, M. Chi and A. T. Bell, *Journal of Catalysis*, 2011, 282, 165-174.
14. X. Fan, J. Li, Z. Zhao, Y. Wei, J. Liu, A. Duan and G. Jiang, *Catal. Sci. Technol.*, 2015, 5, 339-350.
15. O. A. Bariås, A. Holmen and E. A. Blekkan, *J. Catal.*, 1996, 158, 1-12.
16. M. Santhosh Kumar, D. Chen, A. Holmen and J. C. Walmsley, *Catal. Today*, 2009, 142, 17-23.
17. M. Larsson, M. Hultén, E. A. Blekkan and B. Andersson, *J. Catal.*, 1996, 164, 44-53.
18. S. B. Kogan, H. Schramm and M. Herskowitz, *Appl. Catal. A-Gen.*, 2001, 208, 185-191.
19. Z.-J. Sui, Y.-A. Zhu, P. Li, X.-G. Zhou and D. Chen, *Adv. Chem. Eng.*, 2014, 44, 61-125.
20. A. W. Hauser, J. Gomes, M. Bajdich, M. Head-Gordon and A. T. Bell, *Phys.Chem. Chem.Phys.*, 2013, 15, 20727-20734.
21. M.-L. Yang, J. Zhu, Y.-A. Zhu, Z.-J. Sui, Y.-D. Yu, X.-G. Zhou and D. Chen, *Jo. Mol.Catal. A-Chem*, 2014, 395, 329-336.
22. E. H. Lee, *Catal. Rev.*, 1974, 8, 285-305.
23. D. L. Trimm, *Catal. Today*, 1999, 49, 3-10.
24. W. S. Dong, X. K. Wang and S. Y. Peng, *J. Fuel.Chem. Tech.*, 1997, 25, 4.
25. M. Fattahi, F. Khorasheh, S. Sahebdelfar, F. T. Zangeneh, K. Ganji and M. Saeedizad, *Scientia Iranica*, 2011, 18, 1377-1383.
26. Y. Shan, Z. Sui, Y. Zhu, D. Chen and X. Zhou, *Chem. Eng. J.*, DOI: http://dx.doi.org/10.1016/j.cej.2014.09.107.
27. W. S. Dong, H. J. Wang, X. K. Wang and S. Y. Peng, *J. Mol. Catal. (China)*, 1999, 13, 181-185.
28. C. Yu, Q. Ge, H. Xu and W. Li, *Ind.Eng. Chem. Res.*, 2007, 46, 8722-8728.
29. L.C. Luu, N.A. Gaidai, S.L. Kiperman, H. Shi Thoang, Kinet. Catal.,1996, 37, 851–857.
30. S. B. Kogan, H. Schramm and M. Herskowitz, *Appl. Catal. A-Gen.*, 2001, 208, 185-191.
31. Q. Li, Ph.D. Thesis, East China University of Science and Technoloty, 2012.

32. G. Kresse and J. Furthmüller, *J. Comp. Mater. Sci.*, 1996, 6, 15-50.
33. G. Kresse and J. Furthmüller, *J. Phys. Rev. B*, 1996, 54, 11169-11186.
34. G. Kresse and J. Furthmüller, *J. Phys. Rev. B*, 1993, 48, 13115-13118.
35. P. E. Blöchl, *Phys. Rev. B*, 1994, 50, 17953-17979.
36. M. Methfessel and A. T. Paxton, *Phys. Rev. B*, 1989, 40, 6.
37. M.-L. Yang, Y.-A. Zhu, C. Fan, Z.-J. Sui, D. Chen and X.-G. Zhou, *Phys. Chem. Chem. Phys.* 2011, 13, 3257-3267.
38. G. Henkelman and H. Jónsson, *J. Chem.phys.*, 1999, 111, 7010-7022.
39. G. Henkelman and H. Jónsson, *J. Chem.Phys.*, 2001, 115, 9657-9666.
40. R. Olsen, G. Kroes, G. Henkelman, A. Arnaldsson and H. Jónsson, *J. Chem. Phys.*, 2004, 121, 9776-9792.
41. P. Biloen, F. Dautzenberg and W. Sachtler, *J.Catal.*, 1977, 50, 77-86.
42. C. Michel, F. Göltl and P. Sautet, *Phys. Chem. Chem. Phys*, 2012, 14, 15286-15290.
43. S. Chibani, C. Michel, F. Delbecq, C. Pinel and M. Besson, *Catal. Sci. Technol*, 2013, 3, 339-350.
44. P. Tereshchuk and J. L. Da Silva, *J. Phys. Chem. C*, 2013, 117, 16942-16952.
45. K. Chen, A. Khodakov, J. Yang, A. T. Bell and E. Iglesia, *J. Catal*, 1999, 186, 325-333.
46. K. Chen, E. Iglesia and A. T. Bell, *J. Phys.Chem. B*, 2000, 105, 646-653.
47. P. C. Redfern, P. Zapol, M. Sternberg, S. P. Adiga, S. A. Zygmunt and L. A. Curtiss, *J. Phy. Chem. B*, 2006, 110, 8363-8371.
48. M. M. Barsan and F. C. Thyrion, *Catal. Today*, 2003, 81, 159-170.
49. M.-J. Cheng, K. Chenoweth, J. Oxgaard, A. van Duin and W. A. Goddard, *J.of Phys.Chem. C*, 2007, 111, 5115-5127.
50. R. Grabowski, S. Pietrzyk, J. Słoczyński, F. Genser, K. Wcisło and B. Grzybowska-Świerkosz, *Appli. Catal. A-Gen.*, 2002, 232, 277-288.
51. R. Grabowski and J. Słoczyński, *Chemical Engineering and Processing: Process Intensification*, 2005, 44, 1082-1093.
52. Y.-J. Du, Z. H. Li and K.-N. Fan, *J. Mol. Catal. A-Chem.*, 2013, 379, 122-138.
53. G.-L. Dai, Z.-H. Li, J. Lu, W.-N. Wang and K.-N. Fan, *J. Phys. Chem. C*, 2011, 116, 807-817.
54. H. Fu, Z.-P. Liu, Z.-H. Li, W.-N. Wang and K.-N. Fan, *J. Am. Chem. Soc.*, 2006, 128, 11114-11123.
55. F. Gilardoni, A. T. Bell, A. Chakraborty and P. Boulet, *J. Phys. Chem. B*, 2000, 104, 12250-12255.
56. G. L. Dai, Z. H. Li, J. Lu, W. N. Wang and K. N. Fan, *J. Phys. Chem. C*, 2011, 116, 807-817.
57. D. Chen, Proceedings of the 23rd North American Catalysis Society Meeting. Nam, 2013.
58. D. Duprez, M. Hadj-Aissa, J. Barbier, *Appl. Catal.*,1989,49, 67-74.
59. D. Duprez, M. Hadj-Aissa, J. Barbier, *Appl. Catal.*,1989,49, 75-82.
60. C. L. Yu, H. Y. Xu, *Acta Petrolei Sinica(Petroleum Processing Section)*, 2011, 27, 476-481.
61. M.-L. Yang, Y.-A. Zhu, C. Fan, Z.-J. Sui, D. Chen and X.-G. Zhou, *J. Mol. Catal. A-Chem.*, 2010, 321, 42-49.
62. L. Nykänen and K. Honkala, *ACS Catal.*, 2013, 3, 3026-3030.
63. O. A. Bariås, A. Holmen and E. A. Blekkan, *Catal. Today*, 1995, 24, 361-364.
64. E. Jablonski, A. Castro, O. Scelza and S. De Miguel, *Appl. Catal. A-Gen*, 1999, 183, 189-198.

65. A. G. Sault, A. Martino, J. S. Kawola and E. Boespflug, *J. Catal.*, 2000, 191, 474-479.
66. Q. Li, Z. Sui, X. Zhou, Y. Zhu, J. Zhou and D. Chen, *Top.Catal*, 2011, 54, 888-896.
67. G. Aguilar−Ríos, P. Salas, M. A. Valenzuela, H. Armendáriz. J. A. Wang, J. Salmones, *Catal. Lett.*, 1999, 60, 21-25.